Molecular-scale characterization of groundwater treatment sludge from around the world Implications for potential arsenic recovery

Wang, K.; Holm, P. E.; Trettenes, U. Brinkmann; Bandaru, S. R.S.; van Halem, D.; van Genuchten, C. M.

DOI
10.1016/j.watres.2023.120561

Publication date
2023

Document Version
Final published version

Published in
Water Research

Water Research 245 (2023) 120561

Contents lists available at ScienceDirect

Water Research

journal homepage: www.elsevier.com/locate/watres

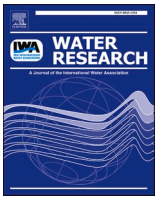

Molecular-scale characterization of groundwater treatment sludge from around the world: Implications for potential arsenic recovery

K. Wang [a], P.E. Holm [b], U. Brinkmann Trettenes [c], S.R.S. Bandaru [d], D. van Halem [e], C.M. van Genuchten [a,*]

[a] Department of Geochemistry, Geological Survey of Denmark and Greenland (GEUS), Øster Voldgade 10, Copenhagen, Denmark
[b] Department of Plant and Environmental Sciences, University of Copenhagen, Thorvaldsensvej 40, 1871 Frederiksberg C, Denmark
[c] VandCenterSyd, Vandvaerkersvej 7, 5000 Odense C, Denmark
[d] University of California, Berkeley, Berkeley, California, USA
[e] Technical University of Delft, Delft, The Netherlands

ARTICLE INFO

Keywords:
Arsenic
Groundwater treatment sludge
Resource recovery
Critical raw materials

ABSTRACT

Iron (Fe)-based treatment methods are widely applied to remove carcinogenic arsenic (As) from drinking water, but generate toxic As-laden Fe (oxyhydr)oxide waste that has traditionally been ignored for resource recovery by the water sector. However, the European Commission recently classified As as a Critical Raw Material (CRM), thus providing new incentives to re-think As-laden groundwater treatment sludge. Before As recovery techniques can be developed for groundwater treatment waste, detailed information on its structure and composition is essential. To this end, we comprehensively characterized sludge generated from a variety of As-rich groundwater treatment plants in different geographic regions by combining a suite of macroscopic measurements, such as total digestions, leaching tests and BET surface area with molecular-scale solid-phase analysis by Fe and As K-edge X-ray absorption spectroscopy (XAS). We found that the As mass fraction of all samples ranged from ~200–1200 mg As/kg (dry weight) and the phosphorous (P) content reached ~0.5–2 mass%. Notably, our results indicated that the influent As level was a poor predictor of the As sludge content, with the highest As mass fractions (940–1200 mg As/kg) measured in sludge generated from treating low groundwater As levels (1.1–22 μg/L). The Fe K-edge XAS data revealed that all samples consisted of nanoscale Fe(III) precipitates with less structural order than ferrihydrite, which is consistent with their high BET surface area (up to >250 m^2/g) and large As and P mass fractions. The As K-edge XAS data indicated As was present in all samples predominantly as As(V) bound to Fe(III) precipitates in the binuclear-corner sharing (^{2}C) geometry. Overall, the similar structure and composition of all samples implies that As recovery methods optimized for one type of Fe-based treatment sludge can be applied to many groundwater treatment sludges. Our work provides a critical foundation for further research to develop resource recovery methods for As-rich waste.

1. Introduction

Approximately 94–200 million people are potentially exposed to carcinogenic arsenic (As) in groundwater at levels above the World Health Organization (WHO) provisional limit of 10 μg/L (Podgorski and Berg, 2020). Many regions already rely heavily on groundwater treatment to meet the 10 μg/L WHO drinking water guideline when access to alternative water sources is not available. However, there is a growing consensus that the 10 μg/L guideline is not low enough to sufficiently protect public health from negative impacts of chronic As exposure (Ersboll et al., 2018). Indeed, several regulatory agencies target As drinking water levels <10 μg/L (Ramsay et al., 2021), with the Netherlands recently aiming for 1 μg/L (Ahmad et al., 2020). Moreover, the California EPA has set a Public Health Goal for As of 4 ng/L (2,500 times lower than the WHO guideline), which is a health-based goal that is thought to reflect actual safe As concentrations in drinking water (Frisbie and Mitchell, 2022). As more regions continue to target increasingly stringent As drinking water limits, the reliance on groundwater treatment is expected to grow.

The most common groundwater treatment methods in both high- and low-income regions are based on As sorption to iron (Fe) (oxyhydr)oxides, but some key differences among these methods exist. Aeration-

* Corresponding author.
E-mail address: cvg@geus.dk (C.M. van Genuchten).

https://doi.org/10.1016/j.watres.2023.120561
Received 9 June 2023; Received in revised form 25 August 2023; Accepted 30 August 2023
Available online 31 August 2023

filtration is one of the simplest methods and is employed in many large-scale conventional groundwater treatment plants (Gude et al., 2016). This method relies on aerating groundwater containing Fe(II) and arsenite (As(III)), the most common form of As in groundwater, to oxidize Fe(II) and produce particulate Fe(III) (oxyhydr)oxides (BGS, 2001; van Genuchten and Ahmad, 2020). The oxidation of Fe(II) by O_2 also creates reactive Fenton-type oxidants that can co-oxidize As(III) to arsenate (As(V)), which binds effectively to Fe(III) precipitates (Hug and Leupin, 2003). The As-laden solids are then separated from treated water with sand filters. The aeration-filtration process can be enhanced by stimulating bacterial growth on sand filters to accelerate Fe(II) and As (III) oxidation, which is often referred to as biological-adsorptive Fe removal (Gude et al., 2018). When naturally-occurring Fe in groundwater is not sufficient to remove As, additional Fe is dosed often via acidic ferric chloride ($FeCl_3$) solution (Hering et al., 1996). However, in decentralized As-affected regions, such as rural India, the production and transport of $FeCl_3$ is a logistical challenge. Therefore, groundwater treatment can rely on the electrolytic dissolution of Fe(0) metal as the source of Fe(III) (oxyhydr)oxides to bind As, which is a technique called Fe(0) electrocoagulation (Bandaru et al., 2020a). The efficiency of Fe(0) electrocoagulation can be enhanced by employing an air-cathode to generate H_2O_2 (i.e., electro-Fenton treatment), which increases the rates of Fe(II) and As(III) co-oxidation (Bandaru et al., 2020b). While each of these methods excel in different conditions (e.g., low vs high influent As levels; small vs large plant capacity; low vs high infrastructure requirements) they all generate solid As-laden sludges that must be managed as part of routine operation.

Due to concerns over As toxicity, As-laden groundwater treatment sludge has traditionally been regarded as a worthless by-product that requires disposal (Clancy et al., 2013), rather than a secondary source of critical materials. Accordingly, previous research on groundwater treatment sludge has focused mainly on characterizing As-free sludge in the context of agricultural application or repurposing as sorption media for water treatment (Keeley et al., 2014; Turner et al., 2019). For example, Likus et al. (2021) investigated the physicochemical and textural properties of sludge derived from aeration-filtration plants for Fe and Mn removal and suggested that the highly porous, nanoscale Fe (III) solids could be ideal for subsequent contaminant removal. Water treatment residuals with similar structures were also proposed to prevent phosphorous (P) runoff from agricultural land following fertilizer application (Gallimore et al., 1999). While these studies on waste reuse are useful, analogous investigations have not been performed on sludge containing As, the presence of which would typically be viewed negatively for reuse applications. However, the societal value of As is currently being redefined. In 2023, As appeared in the European Commission's list of Critical Raw Materials (CRMs; Figure S1 in the Supplementary Materials) due to its widespread use in key products (e.g., batteries, alloys, high-speed electronics) and its global supply being dominated by a single country (European Commission, 2023; Shi et al., 2017). This classification provides increased incentive to upcycle local sources of As, such as As-rich groundwater treatment waste. An essential step to create techniques to convert As-rich waste into valuable materials is to determine the composition and solid-phase As and Fe speciation of different treatment sludges generated around the world.

In this work, we comprehensively characterized As-bearing sludge collected directly from the sludge storage areas of a variety of Fe-based groundwater treatment plants. The investigated plants were selected strategically to include 1) aeration-filtration, 2) biological-adsorptive Fe removal, 3) ferric chloride addition, 4) Fe(0) electrocoagulation and 5) electro-Fenton treatment. In addition, the plants were selected to span wide ranges of capacity (3,650–5,500,000 m^3/y), geographic region (North America, Europe, Asia) and groundwater composition (e.g., influent As levels of 1–390 μg/L). Rather than perform a cursory investigation of more samples, we opted to perform detailed characterization of fewer, but indicative samples. To this end, we combined a suite of macroscopic measurements, such as elemental composition, leaching tests and BET surface area, with molecular-scale solid-phase analysis by synchrotron-based Fe and As K-edge X-ray absorption spectroscopy (XAS). Our study indicates that As-bearing groundwater treatment sludge can be a local source of CRMs (e.g., As, P, Mn) and provides new information to inspire the design of novel As recovery techniques.

2. Materials and methods

2.1. Sludge collection

Arsenic-bearing groundwater treatment sludge was obtained from six separate treatment plants: Holmehave (HH), DK (aeration-filtration); Lunde, DK (aeration-filtration); Kerte, DK (ferric chloride addition); Mol, BE (biological-adsorptive Fe removal); Dhapdhapi, West Bengal, IN (Fe(0) electrocoagulation) and Allensworth, California, USA (electro-Fenton treatment). Key details of each plant are summarized in Table 1, with detailed descriptions of each plant given in Section 1 of the Supplementary Material (SM). Sludge samples (0.5–2 kg) were obtained directly from the sludge storage area of each plant and sealed in air-tight plastic bags or bottles on site. Samples were stored in air-tight containers at room temperature in our laboratory between collection and subsequent processing. The sludge was also dried at room temperature, which reduces the likelihood for structural transformation that might occur at higher drying temperatures. After drying, the solids were homogenized with a mortar and pestle and passed through a 4 mm sieve prior to analysis, consistent with standard sludge characterization protocols (ECS, 2002). The final solids resembled dried powders.

2.2. Sludge composition and surface area

The mass fractions of total dissolvable major and minor elements in the sludge samples were determined by aqua regia digestions. The digestions were performed by adding dried solids to aqua regia solution (3 parts HCl, 1 part HNO_3) at a total solids concentration of 2.0 g/L. Between 2–4 replicate digestions were performed for each sludge sample, with the replicates reflecting separate samples obtained from the same sludge source. We report the average and standard deviation of these replicate digestions in Table 2. The digestion proceeded for 24 h, which is sufficient to dissolve most Fe and Mn (oxyhydr)oxides and carbonates, but might not dissolve robust silicates, such as crystalline quartz (Chen and Ma, 2001). The digestion was then passed through 0.2 μm cellulose acetate filters to remove any recalcitrant solids and diluted 20 times in 2% HNO_3 for subsequent measurements of As, P, Fe, Ca and Mn by inductively-coupled plasma optical emission spectroscopy (ICP-OES). Additional details of the ICP-OES analyses are provided in Section 2 of the SM. The total dissolvable mass fraction is given in mg/kg or g/kg of total sludge dry weight.

The water content and loss on ignition (LOI) were measured following Danish Standard protocols (DS 405.11 and DS 204), using temperatures of 105 and 550 °C for water content and LOI measurements, respectively. Additional details of these measurements are given in the SM. The specific surface area (m^2/g) was measured using the Brunauer-Emmett-Teller (BET) method. For these measurements, approximately 100–200 mg of each sludge sample was degassed at 60 °C for 3.1 h. The measurements were performed with a Micromeritics Gemini VII instrument.

2.3. Standard leaching tests

Two types of leaching tests were performed. The first test was based on the European Union standard for leaching of granular waste materials and sludges (EN 12457-2), which has been adopted in Denmark (ECS, 2002; EN 12457-2, 2002). For this batch test, 5 g of dried and crushed sludge samples were combined with DI water at a ratio of 10 L/kg and mixed with a benchtop shaker for 24 h. After the reaction, the eluate was

Table 1
Properties of Groundwater Treatment Plants.

Name	Treatment Process	Plant Capacity (m^3/y)	Influent As (μg/L)	Effluent pH	Sludge Disposal Method
Holmehave	Aeration-filtration	5,500,000	1.1–12.2	7.3–8.0	Biogas Plant
Lunde	Aeration-filtration	1,000,000	1.4–3.4	7.3–7.9	Biogas Plant
Kerte	Ferric chloride addition	80,000	12–22	7.4–7.9	Pond disposal
Mol	Biological-adsorptive Fe and As removal	3,650,000	36–50	7.9–8.3[A]	Landfill
Dhapdhapi	Electrocoagulation	3,650	250–300	7.5–7.7	Landfill
Allensworth	Electro-Fenton	5,000	130–390	8.0–8.6	Landfill

[A] This pH reflects the effluent after NaOH addition. Treatment plant properties were obtained from standard reports given by treatment plant operators.

Table 2
Chemical composition and surface area of sludge samples.

Sample Name	Chemical Composition[A] and Surface Area								
	As (mg/kg)	Fe (g/kg)	As/Fe (mol%)	P (g/kg)	Ca (g/kg)	Mn (g/kg)	BET (m^2/g)	H_2O[B] Content (%)	LOI (%)
HH	942±29	351±29	0.20	20.0 ± 2.5	42.1 ± 3.1	11.2 ± 0.5	224	23.6	14.3
Lunde	188±58	332±15	0.04	14.4 ± 0.6	41.0 ± 2.9	2.36±0.13	102	24.5	14.8
Kerte	1,199±94	188±8	0.47	17.0 ± 0.5	70.0 ± 4.5	78.7 ± 5.5	134	11.3	12.4
Mol	563±82	422±10	0.10	16.5 ± 0.9	4.93±0.13	0.31±0.01	263	40.2	14.4
Allensworth	864±33	205±8	0.31	–	8.36±0.32	0.16±0.01	92	7.4	9.3
Dhapdhapi	817±42	184±1	0.33	4.9 ± 0.4	94.6 ± 20.2	1.01±0.10	102	6.3	11.6

[A] All element fractions are given in units of mass/total sludge mass dry weight. Aluminum, carbon and oxygen were not measured in the acid digestions, but are expected to be major contributions of the remaining elemental fractions. The – symbol indicates values that were not measured.
[B] Ferrihydrite has a high mass fraction of structural water that can be released during heating (Hiemstra, 2013).

separated from the solids using 0.2 μm cellulose acetate filters and acidified with HNO_3 for subsequent ICP-OES measurements.

The second test was based on the standard leaching procedure applied in the US, the Toxicity Characteristic Leaching Procedure (TCLP) (USEPA, 1992). For this test, a solution of 0.1 M acetic acid and 0.064 M NaOH (pH 4.93) was prepared and 2.5 g of each sludge sample was mixed at a solution-to-solid ratio of 20:1. The suspension was mixed with a benchtop shaker for 18 h, after which the eluate was separated using 0.2 μm cellulose acetate filters and acidified with HNO_3 for ICP-OES measurements.

2.4. X-ray diffraction

Powder X-ray diffraction (XRD) patterns were collected on the solid samples using a Philips X'Pert Pro diffractometer equipped with a rotating sample stage and Co K-alpha radiation. Data were collected from 5 to 70° 2θ with 0.02° step sizes, resulting in total data collection time of ~4 h per sample.

2.5. X-ray absorption spectroscopy

Fe and As K-edge XAS data were collected at the Balder beam line of the MAX IV synchrotron (Lund, Sweden) and at beam line 4–1 of the Stanford Synchrotron Radiation Lightsource (SSRL, Menlo Park, USA). Fe K-edge XAS data were recorded in transmission mode out to k of 12 $Å^{-1}$ at room temperature. As K-edge XAS data were recorded in fluorescence mode out to k of 12–14 $Å^{-1}$ using a liquid nitrogen or helium cryostat. The maximum of the first derivative of Fe(0) and Au(0) foils were set to 7,112 eV (Fe measurements) or 11,919 eV (As measurements) for calibration of the X-ray energy. Two to 10 scans were collected for each sample, depending on data quality. Changes in line shape and peak position indicative of beam damage were examined, but no artifacts were observed. The SixPack software (Webb, 2005) was used to align, average, and background-subtract experimental spectra following standard methods described previously (van Genuchten et al., 2012). The EXAFS spectra were extracted using k^3-weighting and were Fourier-transformed over the k-range 2 to 11 using a Kaiser-Bessel window with dk of 3 $Å^{-1}$.

The Fe K-edge EXAFS spectra were analysed qualitatively by comparison with the spectra of Fe-bearing reference minerals that were collected at the same beam lines with identical data collection procedures. These references included goethite, lepidocrocite and nanocrystalline 2-line ferrihydrite (Fh). Details on the synthesis of these solids can be found elsewhere (Cornell and Schwertmann, 1996; van Genuchten et al., 2014).

The As K-edge XANES spectra were analysed by linear combination fits (LCFs) using the SixPack software to determine the fraction of As(III) and As(V) in each sample. The LCFs were performed over the range of 11,860 to 11,880 eV without constraining the sum of the components to 1. The reference spectra used in the XANES fits included As(III) and As (V) adsorbed to Fh.

The As K-edge EXAFS spectra were analysed by shell-by-shell fits to determine the As coordination environment in the sludge samples. Theoretical curve fits were performed from 1 to 3.5 Å in $R+\Delta R$-space, based on algorithms derived from IFEFFIT (Newville, 2001). The interatomic distance (R), coordination number (CN), mean squared atomic displacement parameter (σ^2) and the change in threshold energy (ΔE_0) were typically varied for each fit. Phase and amplitude functions for single and multiple scattering paths were calculated using FEFF6 (Newville, 2001) and included As-O, As-O-O and As-Fe paths derived from the structure of scorodite (Kitahama et al., 1975). The goodness-of-fit was assessed based on the R-factor, which is defined as the mean square difference between the fit and the data on a point-by-point basis: $R = \sum_i (\text{data}_i - \text{fit}_i)^2 / \sum_i (\text{data}_i)^2$. Additional details of XAS data collection and the shell-by-shell fit analysis are presented in Section 3 of the SM.

3. Results

3.1. Elemental composition and surface area

3.1.1. As mass fractions

The As mass fractions for all samples exceeded 180 mg As/kg (Table 2), but some deviation among the samples was observed. The lowest As mass fraction of 188 mg As/kg was detected for the Lunde treatment plant sludge, which receives a relatively low influent As concentration of 1.1–3.4 μg/L. The sludge samples with the highest As mass fractions of ~1,200 and 940 mg As/kg were collected from the Kerte and Holmehave (HH) treatment plants, respectively. Although Kerte and HH sludge had the highest As contents, the influent As

concentrations to both plants (12–22 μg As/L for Kerte, 1.1–12.2 μg As/L for HH) were only slightly higher than that of the Lunde plant. The conventional treatment plant located in Mol, BE generated sludge with an As mass fraction of 560 mg As/kg, which was intermediate between the three Danish treatment plants despite its higher influent As concentration (36–50 μg As/L). Finally, the two electrochemical treatment plants in this study, Allensworth and Dhapdhapi, generated sludge with similar As contents of 864 and 817 mg As/kg, respectively. The influent As levels into these electrochemical systems were the highest of all investigated plants (130–390 μg As/L for Allensworth, 250–300 μg As/L for Dhapdhapi), but the As sludge content was still lower than solids from the HH and Kerte plants.

3.1.2. Fe mass fractions

The aqua regia digestions revealed that Fe was by far the most concentrated metal in the sludge of all plants, in agreement with the orange-to-brown color of all samples (Figure S2). The Fe content of the sludge varied from ~180–420 g Fe/kg (i.e., 18–42 mass%), which is consistent with the key role of Fe in As removal for these plants. No clear trends in sludge Fe content with treatment plant were apparent. In fact, the treatment plants that do not dose additional Fe (i.e., HH, Lunde, Mol) generated sludge with the highest Fe fractions (330–420 g Fe/kg for these three plants). Consistent with their high Fe content, the Lunde, Mol and HH sludges had the lowest As/Fe mol ratios of 0.04, 0.10 and 0.20 mol%, respectively, whereas the As/Fe ratio of sludge generated from Allensworth, Dhapdhapi and Kerte plants ranged from 0.31 to 0.47 mol%. Further analysis of the As/Fe ratio of raw groundwater and solid sludge for selected treatment plants is given in Section 4 of the SM.

3.1.3. Mass fractions of other elements

In addition to As and Fe, several other elements were present in considerable fractions in the sludge of each plant. In particular, P was detected in all sludge, with the HH solids containing the highest P fraction of 20 g P/kg (2 mass%). The P content also exceeded 14 g P/kg for the Lunde, Kerte and Mol sludge, which was at least 15 times higher than the corresponding As content, consistent with the typically higher concentration of P than As in natural groundwater (e.g., 1–3 mg/L P, 100–300 μg/L As in South Asian groundwater (BGS, 2001)). Calcium was a major fraction of the Kerte (70 g Ca/kg) and Dhapdhapi (95 g Ca/kg) sludge, approximately twice as high as the Ca content of the next highest grouping of sludge (Lunde and HH = 41–42 g Ca/kg). The Dhapdhapi sludge contained roughly half as much Ca as Fe, which is notable due to the large Fe dosage (i.e., several hundred mg Fe/L) used for As removal at this plant (Bandaru et al., 2020a). Finally, Mn was also present in substantial fractions in the sludge generated at Kerte (78.7 g Mn/kg) and HH to lesser extent (11 g Mn/kg). The presence of high Mn could be due to the formation of Mn-bearing solids on filter grains that are removed during filter backwashing.

3.1.4. BET surface area, H_2O content and LOI

The BET surface area of all sludge samples uniformly exceeded 90 m^2/g, consistent with porous and possibly nanocrystalline structures, but some variation among the samples was observed. In particular, the HH (224 m^2/g) and Mol (263 m^2/g) sludge samples exhibited the highest BET surface area, more than twice as high as the Allensworth sample (92 m^2/g). For reference, laboratory-synthesized 2-line ferrihydrite, which is a model nanoscale Fe(III) (oxyhydr)oxide, has a reported BET surface area between 150 and 350 m^2/g (Das et al., 2011; Links et al., 2012; Schwertmann and Cornell, 1991). Consistent with the nanoscale structure suggested by the BET surface area measurements, many of the sludge samples were characterized by a high H_2O content, which is also a common property of nanoscale precipitates. In particular, the Mol sample, which had the highest BET surface area, also had the highest H_2O content of 40%. The Allensworth and Dhapdhapi samples, which had the lowest surface areas, also had the lowest H_2O contents of 6.3 and 7.4%, respectively. The exception to this trend was the Lunde sample, which had a high H_2O content (24.5%) and relatively low specific surface area (102 m^2/g). Finally, the LOI was relatively similar across all sludge samples, ranging from 9.3% (Allensworth) to 14.8% (Lunde).

3.2. Leaching tests

Comparing all measurements for both leaching tests (Table 3) revealed that every sludge sample leached As well below the threshold to be considered hazardous waste. For example, no sample leached more than 0.25 mg/L As in the EN 12457-2 test, which meets the 0.5 mg/L criterion to qualify as inert waste (ECS, 2002). Similarly, no sample leached more than 0.3 mg/L As in the TCLP test, falling far below the 5.0 mg/L hazardous waste threshold (USEPA, 1992). Although some small variability in As released from different samples was observed (Table 3), the results of these standard tests suggest comparably low As leaching behavior for all samples and that all sludge solids can be accepted by ordinary municipal landfills. However, it is important to note that standard leaching tests have been widely criticized for underestimating the quantity of toxic species leached from sludge in real landfill conditions (deLemos et al., 2006; Ghosh et al., 2004), and thus are used here primarily to compare leaching properties between samples.

Outside of As, some key ions displayed great variation in the leaching tests. In particular, Ca was released at tens to hundreds of mg/L, depending on the treatment plant and leaching test, which contrasted the minimal leaching of P (<0.06 mg/L for in all samples). For example, the waste collected from Mol waterworks released 13.8 mg/L Ca in the EN 12457–2 test and 138 mg/L Ca in the TCLP test. These values were significantly lower than the Ca leached from the Kerte (EN 12457–2 = 108 mg/L Ca; TCLP = 820 mg/L) and Dhapdhapi (EN 12457–2 = 214 mg/L Ca; TCLP = 954 mg/L) sludges. In general, Ca released by each sample increased with the Ca content of the waste and is consistent with the dissolution of carbonate minerals during the leaching test. Finally, the Kerte sample also had an outlying Mn concentration in the leachate of the TCLP test compared to the other samples (Kerte sludge also contained the highest Mn content, Table 2).

3.3. X-ray diffraction

For most samples, including HH, Lunde and Mol, the XRD patterns (Fig. 1) displayed broad and diffuse scattering fingerprints characteristic of poorly-ordered Fe(III) (oxyhydr)oxides akin to Fh (e.g., low amplitude peak near 38° 2θ). The exceptions were the Kerte and Dhapdhapi samples, which both contained Bragg diffraction peaks from a variety of minerals. For the Kerte sample, the XRD pattern contained intense peaks from quartz and less intense peaks from calcite. In addition, this sample displayed a small, broad peak near 36° 2θ that matches the major peak from the Ca- and Mg-bearing carbonate mineral, dolomite. The quartz, calcite and dolomite peaks in the XRD of the Kerte sample likely reflect both the release of grains from the sand filter during backwashing, combined with the mixture of the concentrated Fe-rich backwash solids with natural sediment at the bottom of the sludge discharge pond where the samples were obtained. For the Dhapdhapi sample, which was generated at an Fe(0) electrocoagulation treatment plant, the XRD pattern also showed evidence for quartz and calcite, but calcite had the most intense peaks. The presence of quartz in this sample can be explained by sand grains originating from the sludge drying bed, but the large component of calcite is most likely due to electrochemical reactions and groundwater composition unique to this treatment plant. Specifically, the cathodic reduction of H^+ to form $H_{2(g)}$ during Fe(0) electrocoagulation treatment creates regions of high pH near the cathode, leading to conditions that favor $CaCO_3$ formation (Muller et al., 2019). While the Kerte and Dhapdhapi samples had some Bragg diffraction peaks of Si- and Ca-bearing minerals, it is noteworthy that none of the samples contained Bragg diffraction peaks for crystalline Fe

Table 3
Summary of leaching results.

Sample Name	EN 12457-2					TCLP				
	As (mg/L)	Fe (mg/L)	P (mg/L)	Ca (mg/L)	Mn (mg/L)	As (mg/L)	Fe (mg/L)	P (mg/L)	Ca (mg/L)	Mn (mg/L)
HH	0.178	DL	DL	54.5	DL	0.160	DL	DL	648	0.201
Lunde	0.107	0.010	DL	57.6	DL	0.237	0.007	DL	661	0.235
Kerte	0.112	DL	0.024	108	0.397	0.017	DL	0.052	820	15.5
Mol	DL	DL	0.023	13.8	0.083	0.011	0.13	0.021	138	4.5
Allensworth	DL	DL	–	43.2	0.024	–	–	–	–	–
Dhapdhapi	0.121	DL	DL	214	0.014	0.134	DL	DL	954	0.626

DL represents the detection limit of the ICP-OES instrument, see SM for additional details. The – symbol indicates values that were not measured. The TCLP test for the Allensworth test was not performed due to insufficient sample material.

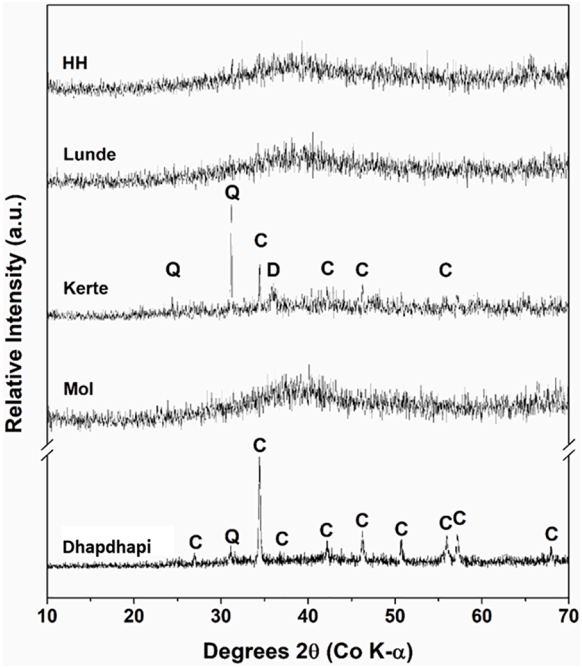

Fig. 1. X-ray diffraction patterns of sludge samples. The peaks identified by Q, C and D represent quartz, calcite and dolomite, respectively.

(oxyhydr)oxides. All sludge samples lacked XRD peaks from common Fe (III) minerals, such as goethite (Goe), lepidocrocite (Lp) and hematite, suggesting that the Fe contained in the solids exists as a poorly-crystalline phase.

3.4. Fe K-edge X-ray absorption spectroscopy

The Fe K-edge EXAFS spectra and corresponding Fourier transforms of the sludge samples are compared to Fe-bearing reference minerals in Fig. 2. Despite the variety of treatment processes used to generate the different sludge samples, all experimental Fe K-edge EXAFS spectra exhibited features consistent with Fh. In particular, the first oscillation of all sample spectra from 3 to 5 $Å^{-1}$ was round and symmetric, which matches this oscillation for Fh, but contrasts the asymmetric oscillation of Lp and the flattened oscillation of Goe. In addition, the sample spectra are all characterized by generally less intense and more broad oscillations at $k > 8$ $Å^{-1}$, which is a better match to the Fh spectrum than Lp or Goe. Some small deviations in the EXAFS spectra among the samples are present, but these subtle differences suggest a small difference in Fe-Fe polymerization rather than a change in major Fe phase.

The Fourier-transformed EXAFS spectra of the experimental samples further support the predominance of poorly-ordered Fe(III) precipitates. While the first-shell Fe-O peak of the experimental samples matches the position of the Fe-O peak of the three reference minerals, consistent with octahedral FeO_6, the relative amplitude of the second-shell peak of the experimental samples is a better match to that of Fh. The second shell of each experimental sample is defined by a broad and relatively symmetric peak with a maximum intensity at the same position as the edge-sharing Fe-Fe atomic pair (Fe-Fe_E) of Goe and Lp. In contrast to the second-shell peak of Goe, which has a major contribution from corner-sharing Fe-Fe octahedra (Fe-Fe_C), the Fe-Fe_C contribution of the experimental samples is highly diminished or altogether absent. Therefore, the major atomic pair giving rise to the second-shell peak of the sludge samples is Fe-Fe_E. However, the intensity of this Fe-Fe_E peak in the sludge samples is lower than that of Fh (Fig. 2C), which implies that the sludge samples have an even lower degree of crystallinity than nanoscale Fh.

3.5. As K-edge X-ray absorption spectroscopy

3.5.1. XANES spectra

All samples were characterized by a XANES absorption maximum that matches the position of the As(V) reference spectra (Fig. 3), indicating the predominance of As(V). However, the Mol sludge exhibited a small shoulder at lower X-ray energy that overlaps with the As(III) reference spectrum, suggesting a minor As(III) fraction. Linear combination fits (LCFs) using the references of As(III) and As(V) adsorbed to Fh verified that most of the sludge samples consisted of negligible quantities of As(III) (values given in% in Fig. 3A). While the XANES LCFs revealed that As(V) was the predominant oxidation state in all sludge samples, both the Mol (16%) and Dhapdhapi (7%) samples contained non-negligible As(III) fractions.

3.5.2. EXAFS spectra

The As K-edge EXAFS spectra and corresponding Fourier transforms of the sludge samples are plotted below As-bearing reference spectra in Fig. 3B and C. The phase and line shape of the major EXAFS oscillations of all sludge samples are similar and match well with those of the reference spectrum of As(V) adsorbed to Fh (As(V)-Ads-Fh). For example, the first oscillation from 3.3 to 5.8 $Å^{-1}$ for the samples is symmetric and broad and the second oscillation from 6.0 to 8.2 $Å^{-1}$ has a shoulder of lower amplitude at lower k. These features are present in the As(V)-Ads-Fh spectrum, but contrast the spectrum of As(V) adsorbed to MnO_2, which is characterized by a narrow first oscillation and a second oscillation with a shoulder of lower amplitude at higher k.

3.5.3. Shell-by-shell fits

The shell-by-shell fit output is overlain on the sample and reference spectra in Fig. 3, with Table 4 providing a summary of the fitting results. Consistent with the similar line shape and phase of all experimental EXAFS spectra, the shell-by-shell fitting results were comparable for all samples and were an excellent match to the fits of As(V)-Ads-Fh. For example, the first-shell peak of all sludge samples was fit with an As-O path with interatomic distance (R_{As-O}) of 1.67–1.69 Å and coordination number (CN_{As-O}) of 4.1–4.4. These values are consistent with As(V) in tetrahedral coordination (Waychunas et al., 1993) and are identical

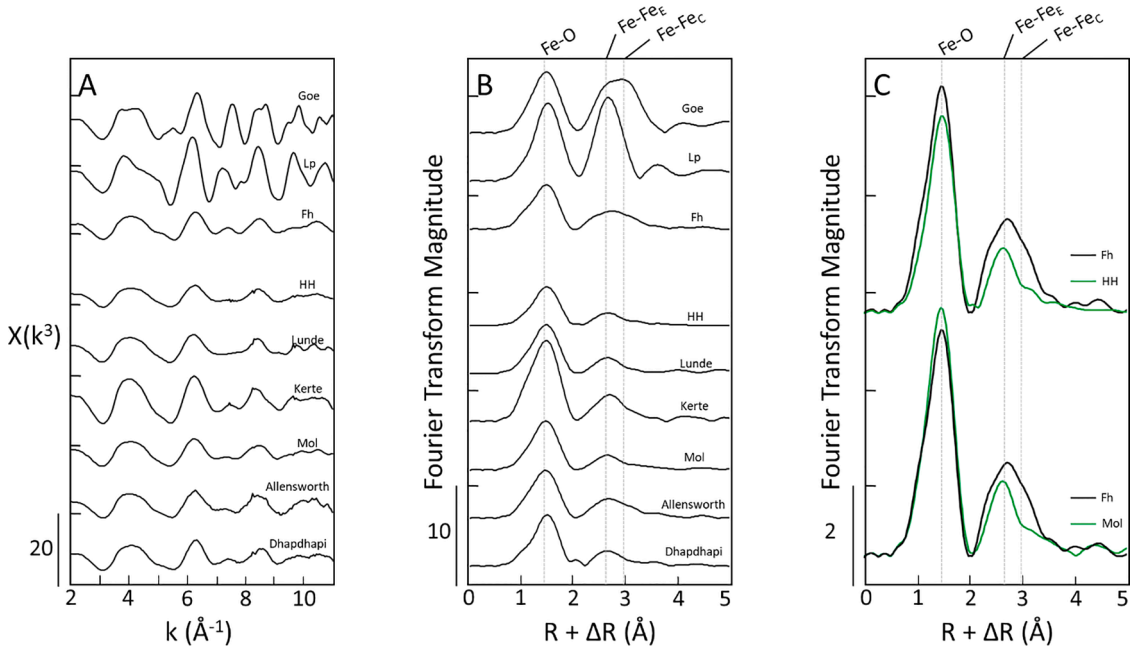

Fig. 2. Fe K-edge EXAFS spectra (A) and corresponding Fourier transforms (B, C) of reference minerals and sludge samples. Panel C compares the Fourier transforms of the HH and Mol sludge with that of the nanocrystalline mineral, Fh. The vertical lines in panels B and C correspond to peaks due to Fe-O, edge-sharing Fe-Fe ($Fe\text{-}Fe_E$) and corner-sharing Fe-Fe ($Fe\text{-}Fe_C$) atomic pairs.

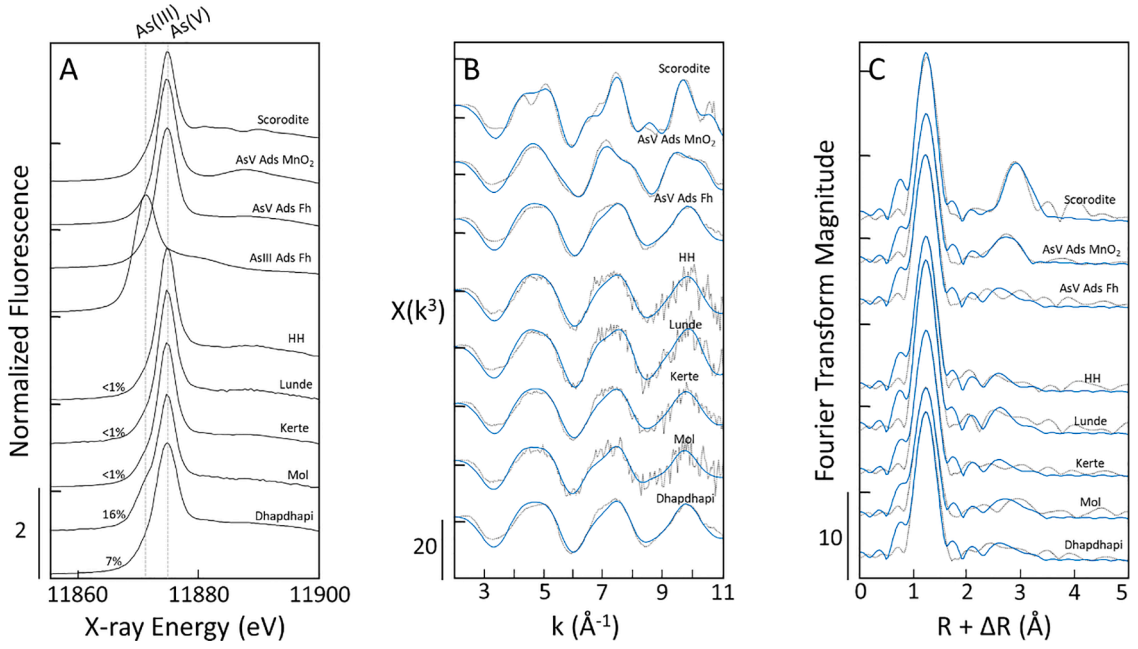

Fig. 3. As K-edge XANES spectra (A), EXAFS spectra (B) and corresponding Fourier-transforms (C) of sludge samples compared to As-bearing reference spectra. The values given in% in panel A represent the fraction of As(III) bound to the solids derived from XANES LCFs. In panels B and C, the output of shell-by-shell EXAFS fits (solid blue lines) is overlain on the data (dotted black lines).

within fit-derived standard errors to the $R_{As\text{-}O}$ (1.67±0.01 Å) and $CN_{As\text{-}O}$ (4.5 ± 0.7) of As(V)-Ads-Fh (Table 4). The Mol sludge had a slightly longer $R_{As\text{-}O}$ (1.69±0.01 Å) than the other samples (1.67–1.68 Å), which is attributed to the minor fraction of As(III) (16% from XANES LCFs) present in this sample and the longer $R_{As\text{-}O}$ of As(III) (~1.78 Å) than As (V) (van Genuchten, 2022).

The fits of the second-shell peak of the experimental samples were all consistent with As(V) bound primarily in the binuclear corner-sharing sorption geometry to Fe(III) precipitates based on the fit-derived $R_{As\text{-}Fe}$ and $CN_{As\text{-}Fe}$ values. Previous EXAFS studies report that Fe(III) (oxyhydr) oxides can bind As(V) in three possible inner-sphere complexes, each with a unique $R_{As\text{-}Fe}$ (Figure S3): 2.9–3.0 Å for the mononuclear edge-sharing (^{1}E) complex; 3.2–3.3 Å for the binuclear corner-sharing (^{2}C) complex; and 3.6–3.7 Å for the mononuclear corner-sharing (^{1}C) complex (Fendorf et al., 1997; Mikutta et al., 2010; Sherman and Randall, 2003; Waychunas et al., 1993). Good quality fits of the second shell for all sludge samples and the As(V)-Ads-Fh reference spectrum were achieved using an As-Fe path with $R_{As\text{-}Fe}$ of 3.24–3.32 Å, which agrees well

Table 4
Shell-by-shell fitting results for references and experimental samples.

Sample	Atomic Pairs	CN	R (Å)	σ^2 (Å^2)	ΔE_0 (eV)	R-Factor
Scorodite	As-O	4.2 (0.6)	1.68 (0.01)	0.002 (0.001)	2.8 (1.7)	0.029
	As-O-O[A]	12	1.82(R_{AsO}) = 3.05	σ^2 (AsO)		
	As-Fe	3.8 (0.5)	3.35 (0.01)	0.004		
As(V) Adsorbed MnO_2	As-O	4.4 (0.6)	1.68 (0.01)	0.003 (0.001)	2.1 (1.8)	0.028
	As-O-O	12	1.82(R_{AsO}) = 3.06	σ^2 (AsO)		
	As-Mn	1.9 (0.4)	3.12 (0.02)	0.005		
As(V) Adsorbed Fh	As-O	4.5 (0.7)	1.67 (0.01)	0.003 (0.001)	1.4 (2.2)	0.040
	As-O-O	12	1.82(R_{AsO}) = 3.04	σ^2 (AsO)		
	As-Fe	1.9 (1.1)	3.27 (0.04)	0.01		
HH	As-O	4.3 (0.6)	1.68 (0.01)	0.002 (0.001)	2.0 (2.0)	0.032
	As-O-O	12	1.82(R_{AsO}) = 3.05	σ^2 (AsO)		
	As-Fe	1.5 (1.0)	3.27 (0.04)	0.01		
Lunde	As-O	4.4 (0.6)	1.67 (0.01)	0.001 (0.001)	1.1 (2.9)	0.027
	As-O-O	12	1.82(R_{AsO}) = 3.05	σ^2 (AsO)		
	As-Fe	2.6 (1.0)	3.24 (0.03)	0.01		
Kerte	As-O	4.2 (0.6)	1.68 (0.01)	0.003 (0.001)	2.6 (1.8)	0.030
	As-O-O	12	1.82(R_{AsO}) = 3.06	σ^2 (AsO)		
	As-Fe	1.4 (0.9)	3.30 (0.04)	0.01		
Mol	As-O	4.4 (0.7)	1.69 (0.01)	0.004 (0.001)	1.9 (2.1)	0.041
	As-O-O	12	1.82(R_{AsO}) = 3.07	σ^2 (AsO)		
	As-Fe	2.5 (1.0)	3.32 (0.03)	0.01		
Dhapdhapi	As-O	4.3 (0.6)	1.68 (0.01)	0.003 (0.001)	1.6 (1.9)	0.032
	As-O-O	12	1.82(R_{AsO}) = 3.05	σ^2 (AsO)		
	As-Fe	1.9 (0.9)	3.30 (0.04)	0.01		

[A] The distance of multiple scattering from As-O-O (CN = 12 for As(V)) was constrained geometrically to single scattering for As-O ($R_{As\text{-}O} = 1.82*R_{As\text{-}O}$). Fitting parameters that were allowed to float are accompanied by fit determined standard errors in parenthesis, whereas constrained parameters are written without parentheses.

with the theoretical $R_{As\text{-}Fe}$ of the ^{2}C As(V) sorption geometry. The fits yielded an even tighter grouping of $R_{As\text{-}Fe}$ values for the samples and As (V)-Ads-Fh reference spectrum (3.24–3.30 Å), if the Mol sample is excluded. The Mol sample had a slightly longer $R_{As\text{-}Fe}$ (3.32±0.03 Å) than the other samples, which is consistent with the presence of a small As(III) fraction. While the fit-derived $CN_{As\text{-}Fe}$ of some sludge samples was slightly lower than the theoretical value of 2 for the ^{2}C geometry, the $CN_{As\text{-}Fe}$ for all samples matched 2 when considering fit-derived uncertainty (e.g., $CN_{As\text{-}Fe}$ for Kerte was 1.4 ± 0.9).

4. Discussion

4.1. Sludge composition: As mass fraction decoupled from influent As concentration

The digestions of sludge samples indicated that all solids contained relatively high As mass fractions of ~200–1200 mg As/kg. One of the key aspects of the measured range of sludge As levels was that the influent As concentration was a poor predictor of the sludge As content. The decoupling of groundwater As concentration and sludge composition is depicted graphically in Fig. 4, which shows that the highest As mass fractions (HH = 942±29 mg As/kg; Kerte = 1199±29 mg As/kg) were detected in sludge generated at plants with some of the lowest influent As concentrations (HH = 1.1–12.2 μg/L; Kerte = 12–22 μg/L). Notably, this decoupling suggests that high As sludge contents are not constrained to facilities treating groundwater with intense As contamination. Rather, high sludge As contents can occur even in cases of low influent As levels. While it is beyond the scope of this study to identify the exact parameters controlling the As content of groundwater treatment waste, the As mass fraction is expected to depend on a combination of several factors, including: 1) the concentration of solid-forming solutes (e.g., Fe, Mn, Ca, etc.) in raw groundwater, which is likely a key governing parameter, 2) the presence of competing species, such as P, silicate (Si) and dissolved organic carbon, 3) pH changes during treatment (Raven et al., 1998) and 4) treatment plant design and operational efficiency (i.e., optimized Fe addition avoids overdosing and leads to lower sludge volume with higher As content).

Among the other components of the sludge, the presence of P is particularly important due partly to its high mass fraction (4.9–20 g P/kg). Groundwater contaminated by As frequently contains P concentrations that exceed As by 1–2 orders of magnitude (BGS, 2001; Smedley and Kinniburgh, 2002). Since PO_4^{3-} and AsO_4^{3-} oxyanions exhibit remarkably similar chemical properties, including pH-dependent charge and tetrahedral shape, P is well known to effectively compete with As for Fe(III) precipitate surfaces by binding in inner-sphere complexes to the same sorption sites as As (Kraal et al., 2019). Consistent with this competition, the P mass fraction of all sludges ranged from ~6–75 times higher than that of As. Therefore, groundwater treatment sludge can be a candidate for resource recovery due to its high P content since P is a CRM (similar to As) and valuable component of fertilizers needed to sustain global food supplies (Alewell et al., 2020). Finally, since Mn is

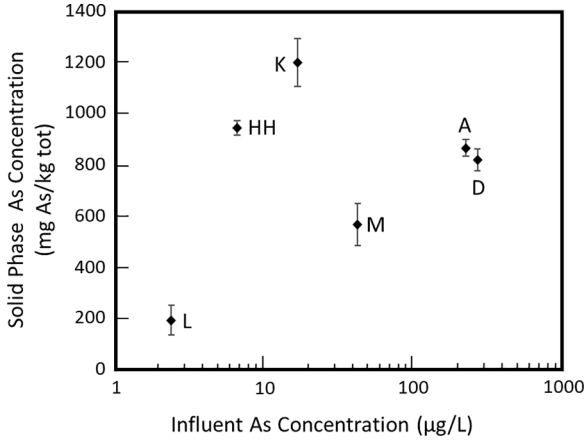

Fig. 4. Solid phase As concentration in mg As/kg in sludge samples plotted as a function of the influent As concentration entering each respective treatment plant. The data points represent the average groundwater As level from the range reported in Table 1 and the average of replicate sludge composition measurements (vertical error bars give the standard deviation of multiple sludge samples for each plant). The letters next to each data point represent Lunde (L), Holmehave (HH), Kerte (K), Mol (M), Allensworth (A) and Dhapdhapi (D).

also classified by the European Commission as a CRM, it is worth noting briefly that Mn was detected in the sludge up to 7.8 mass%. This relatively high Mn content suggests that groundwater treatment sludge can also be a local source of Mn. However, before reliably assessing the potential for Mn recovery from groundwater treatment waste, it is essential to first identify the solid-phase Mn speciation because each potential Mn host phase can have different properties that are relevant for separation and valorisation (e.g., MnO_2 can be reduced readily to form aqueous Mn(II), whereas Mn(II) can be liberated from carbonate minerals by acidic dissolution). Characterizing the Mn speciation in groundwater treatment waste was beyond the scope of the current study but is the subject of our ongoing work.

4.2. Solid-phase speciation of As and Fe in the sludge

The sludge investigated in this work was generated at treatment plants with widely varying As removal processes, including aeration-filtration, ferric chloride addition, biological-adsorptive Fe removal, Fe(0) electrocoagulation and electro-Fenton treatment. Yet, the structural characterization data revealed that the Fe and As bonding modes in all sludges were similar. For Fe, the Fe K-edge EXAFS data, XRD and BET measurements were consistent with the predominance of nano-scale Fe(III) precipitates with structures akin to Fh. The absence of crystalline Fe(III) (oxyhydr) oxides in all sludges can be attributed partly to the composition of the groundwater. In all investigated treatment plants, Fe(III) precipitates are formed in the presence of strongly-sorbing solutes present in groundwater, such as As, P, Si and organic carbon. This formation pathway generates particularly disordered Fe(III) precipitates because strongly-sorbing solutes bind to freshly-generated Fe(III) precipitate surfaces and poison the mineral surface, which inhibits crystallization (Mikutta et al., 2010; Senn et al., 2015; Voegelin et al., 2013). The overall structural impact is the stabilization of nanoscale Fe(III) (oxyhydr)oxides with large reactive surface areas, consistent with the high P and As mass fractions and large BET surface area of the sludge samples. A secondary explanation for the predominance of nanoscale Fe(III) precipitates is most relevant to electro-Fenton treatment and relates to the kinetics of Fe(II) oxidation. The formation of moderately-crystalline Lp from Fe(II) oxidation has been shown to occur via Fe(II)-mediated crystallization of freshly-generated Fe(III) precursors (Sheng et al., 2020). However, electro-Fenton treatment is based on electrochemical formation of Fe(II) and H_2O_2 (Bandaru et al., 2020b), which react orders of magnitude faster than Fe(II) and O_2, preventing the accumulation of aqueous Fe(II) and thus minimizing Fe(II)-mediated crystallization of Fe(III) (oxyhydr)oxides (Roy et al., 2022). While precipitate formation conditions in the investigated plants favor nanoscale solids, the absence of crystalline Fe phases in the sludge is still somewhat surprising considering the sludge handling procedures. In all cases, the solid samples were collected from sludge storage or dewatering areas that often consisted of open-air sand basins exposed to the environment. The aging and drying of nanoscale Fe(III) precipitates is well known to promote Fe phase crystallization and concomitant loss of reactive surface area (Senn et al., 2017). However, we found no evidence for significant crystallization in sludge collected from these storage areas, which points to the strong impact of surface-poisoning solutes on the rates of Fe phase crystallization during aging.

With respect to solid-phase As speciation, the As K-edge XANES LCFs indicated As(V) was the major As oxidation state in all samples, consistent with effective oxidation of As(III), the dominant As form in reduced groundwater aquifers. The oxidation of As(III) in the investigated plants can occur via several mechanisms, including 1) co-oxidation with Fe(II) via powerful Fenton-type oxidants generated by Fe(II) reactions with O_2 or H_2O_2, 2) biologically-catalysed oxidation (e.g., in sand filters), 3) reactions with solid-phase MnO_2, if present and 4) potentially during open-air storage of the sludge (Gude et al., 2018; Hug and Leupin, 2003; Villalobos et al., 2014). However, the presence of As(III) detected in the Mol sludge sample suggests that exposure to the atmosphere during sludge storage might not lead to complete As(III) oxidation. Another similarity among all samples was that As(V) was found by EXAFS spectroscopy to be bound primarily in the same ^2C complex to Fe(III) precipitates. Although some samples, especially Kerte, contained high Mn content (7.8 mass% Mn), the shell-by-shell fits were inconsistent with As(V) bound to MnO_2, which would have a significantly shorter second-shell As-metal interatomic distance (3.12 Å) than what was detected in this sample (3.30 Å, Table 2). The similar As(V) sorption mode among all samples is consistent with the comparable As leaching results (Table 3), with all samples defined as inert by standard leaching tests (despite the detection of some leached As). Overall, the identification of similar As and Fe solid-phase speciation in all sludges, regardless of treatment mechanism, influent groundwater composition and plant capacity, suggests that research to optimize waste management procedures for one type of As-rich sludge can be applied widely to sludge from various Fe-based As treatment methods.

4.3. Benefits of replacing groundwater sludge disposal with advanced As recovery

In this work, we found that As treatment sludge generated from a variety of Fe-based treatment plants in different regions contained As mass fractions of several hundred to over 1000 mg As/kg, even in cases with low groundwater As levels. For comparison, these As mass fractions are only ~10–50 times lower than some raw As mineral ores (Ozer, 2022; Wu et al., 2016) and match or exceed the soil As content of notoriously contaminated Superfund sites (e.g., 100–500 mg As/kg at the Vineland Chemical Company Superfund site, New Jersey, USA; 100–2000 mg As/kg at the Collstrop wood preservation site, Hillerød, DK) (Nielsen et al., 2010; Wovkulich et al., 2010). The disposal of this sludge is an ongoing challenge for treatment operators due partly to its high As content, which makes reuse (e.g., in agricultural applications) impossible. For example, several of the investigated plants landfill the treatment sludge, which is by the far the most common As-rich waste disposal practice in high-income regions (Clancy et al., 2013; Sullivan et al., 2010), despite the inherent drawbacks of this approach (van Genuchten et al., 2022). While As-rich sludge is currently viewed as a disposal challenge in much of the water treatment sector, As is also classified as a Critical Raw Material (CRM) by the European Commission. Along with this classification, the European Commission's 2023 Critical Raw Materials Act specifies benchmarks for domestic As supplies that must be met by 2030 (i.e., ≥10% from extraction, ≥40% from processing, ≥15% from recycling).

Our results suggest that sludge generated from Fe-based As treatment can be a candidate for As recovery, which will help create local sources of CRMs, in agreement with the Critical Raw Materials Act. While not currently practiced, advanced As recovery from As treatment sludge can provide several key benefits. First, As-rich waste disposal via landfilling (high-income areas), sewer discharge, or open disposal to soils and surface water (low-income areas) has been reported to lead to unacceptable toxicity impacts from As emissions to the environment (Le et al., 2022; van Genuchten et al., 2022). Second, the disposal of this waste leads to the loss of As and other CRMs, especially the eutrophying-nutrient P, which was present in the sludge at levels up to 2 mass%. This P mass% is important because it matches the P content reported for dried sewage sludge, which has been the subject of intense resource recovery research in the last decade (Mayer et al., 2016), and 2 mass% is the threshold used by some regulatory agencies to mandate P recovery (Sichler et al., 2022). Third, current methods to produce As compounds, which are based on mining and concentrate processing of As mineral ore, are notoriously damaging to the environment, with large fractions of excavated As emitted to soils nearby mining processing facilities (Shi et al., 2017). Therefore, new (electro)chemical or biological methods able to convert As-rich treatment sludge into valuable As compounds would simultaneously decrease the environmental impacts of current sludge disposal methods, while creating local sources of

CRMs, which would also lessen the reliance on environmentally degrading mining practices.

The observation that sludge generated from several different As treatment methods all contained similar As and Fe solid-phase speciation (i.e., As(V) bound in the ^{2}C geometry to poorly-ordered Fe(III) precipitates) can be useful for the design of subsequent recovery methods. For example, the extraction of As from the sludge, which is likely required before subsequent processing to generate As compounds, is expected to be effective using a reductant to solubilize Fe or by increasing pH to separate As(V) from the negatively-charged Fe(III) precipitate surface. If As(V) were found to bind to a Ca-bearing solid in the sludge, such as $CaCO_3$, a different set of extraction procedures would be effective. For example, mildly acidic conditions can dissolve $CaCO_3$, thus leading to As(V) mobilization. However, mildly acidic conditions can improve As(V) uptake to Fe(III) precipitates compared to circumneutral or alkaline solutions, which demonstrates the strong dependence of As recovery on the As host phase. The development of such methods to recover As and create a circular economy for As-rich sludge can be a breakthrough in *closing the loop* for groundwater treatment, which will likely be of growing importance given the expected reliance on groundwater treatment to meet increasingly stringent As drinking water targets in the future (e.g., 1 μg/L in The Netherlands) (Ahmad et al., 2020).

5. Conclusions

This work systematically studied the basic properties of six As-bearing sludge samples collected from Fe-based groundwater treatment plants with different As removal processes located in Europe, Asia and North America. The As and P mass fractions reached above 1000 mg As/kg and 20 g P/kg, respectively. The highest As contents of 940–1200 mg As/kg were collected from plants with low influent As concentrations (1.1–22 μg/L), indicating that the groundwater As concentration was a poor predictor of the sludge As mass fraction. XRD and Fe K-edge XAS data revealed that all sludge samples consisted of highly-disordered Fe(III) (oxyhydr)oxides, which is attributed to strongly-sorbing groundwater solutes inhibiting Fe(III) precipitate crystal growth. In all samples, As was present predominantly as As(V) bound in the binuclear corner-sharing (^{2}C) geometry to poorly-ordered Fe(III) (oxyhydr)oxides. Despite differences in treatment mechanism, influent groundwater composition and plant capacity, the structural consistency of Fe and As in the sludge suggests that research to optimize resource recovery from one type of sludge can be extended to various Fe-based As treatment methods.

Declaration of Competing Interest

The authors declare that they have no known competing financial interests or personal relationships that could have appeared to influence the work reported in this paper.

Data availability

Data will be made available on request.

Acknowledgements

This work was supported by a Start-up Grant from GeoCenter Denmark and by a Project1 Grant (Thematic Research for the Green Transition) from the Independent Research Fund Denmark (project no. 1127-00207B). We gratefully acknowledge the useful comments provided by an anonymous reviewer during peer review that improved this work. Ryan Davis at SSRL and Kajsa Sigfridsson Clauss at MAX IV are thanked for support during XAS data collection. Use of SSRL, SLAC National Accelerator Laboratory, was supported by the U.S. Department of Energy, Office of Science, Basic Energy Sciences, under Contract No. DE-AC02-76SF00515. We acknowledge MAX IV Laboratory for time on the Balder beam line under Proposal 20221096. Research conducted at MAX IV, a Swedish national user facility, is supported by the Swedish Research Council under contract 2018-07152, the Swedish Governmental Agency for Innovation Systems under contract 2018-04969, and Formas under contract 2019-02496.

Supplementary materials

Supplementary material associated with this article can be found, in the online version, at doi:10.1016/j.watres.2023.120561.

References

Ahmad, A., van der Wens, P., Baken, K., et al., 2020. Arsenic reduction to <1microg/L in Dutch drinking water. Environ. Int. 134, 105253.
Alewell, C., Ringeval, B., Ballabio, C., et al., 2020. Global phosphorus shortage will be aggravated by soil erosion. Nat. Commun. 11.
Bandaru, S.R.S., Roy, A., Gadgil, A.J., et al., 2020a. Long-term electrode behavior during treatment of arsenic contaminated groundwater by a pilot-scale iron electrocoagulation system. Water Res. 175, 115668.
Bandaru, S.R.S., Van Genuchten, C.M., Kumar, A., et al., 2020b. Rapid and efficient arsenic removal by iron electrocoagulation enabled with in situ generation of hydrogen peroxide. Environ. Sci. Technol. 54, 6094–6103.
BGS, 2001. Arsenic Contamination of Groundwater in Bangladesh. British Geological Survey. Tech. Rep. WC/00/19.
Chen, M., Ma, L.Q., 2001. Comparison of three aqua regia digestion methods for twenty Florida soils. Soil Sci. Soc. Am. J. 65, 491–499.
Clancy, T.M., Hayes, K.F., Raskin, L., 2013. Arsenic waste management: a critical review of testing and disposal of arsenic-bearing solid wastes generated during arsenic removal from drinking water. Environ. Sci. Technol. 47, 10799–10812.
Cornell, R.M., Schwertmann, U.C.N.-J., 1996. The Iron Oxides : Structure, Properties, Reactions, Occurrence, and Uses. VCH, Weinheim, New York, p. 1996.
Das, S., Hendry, M.J., Essilfie-Dughan, J., 2011. Transformation of two-line ferrihydrite to goethite and hematite as a function of pH and temperature. Environ. Sci. Technol. 45, 268–275.
deLemos, J.L., Bostick, B.C., Renshaw, C.E., et al., 2006. Landfill-stimulated iron reduction and arsenic release at the Coakley Superfund Site (NH). Environ. Sci. Technol. 40, 67–73.
ECS, 2002. Characterization of Waste, Compliance Test for Leaching of Granular Wastes Materials and Sludges, Part 2. European Committee of Standardization (ECS), CEN/TC 292, 12/02/2002.
EN 12457-2, 2002. Characterisation of Waste - Leaching - Compliance Test for Leaching of Granular Waste Materials and Sludges - Part 2: One Stage Batch Test at a Liquid to Solid Ratio of 10 l/kg for Materials with Particle Size Below 4mm.
Ersboll, A.K., Monrad, M., Sorensen, M., et al., 2018. Low-level exposure to arsenic in drinking water and incidence rate of stroke: a cohort study in Denmark. Env. Int. 120, 72–80.
European Commission, 2023. Study on the Critical Raw Materials for the EU.
Fendorf, S., Eick, M.J., Grossl, P., et al., 1997. Arsenate and chromate retention mechanisms on goethite .1. Surface structure. Environ. Sci. Technol. 315–320.
Frisbie, S.H., Mitchell, E.J., 2022. Arsenic in drinking water : an analysis of global drinking water regulations and recommendations for updates to protect public health 17, 1–42.
Gallimore, L.E., Basta, N.T., Storm, D.E., et al., 1999. Water treatment residual to reduce nutrients in surface runoff from agricultural land. J. Environ. Qual. 28, 1474–1478.
Ghosh, A., Mukiibi, M., Ela, W., 2004. TCLP underestimates leaching of arsenic from solid residuals under landfill conditions. Environ. Sci. Technol. 4677–4682.
Gude, J.C.J., Joris, K., Huysman, K., et al., 2018. Effect of supernatant water level on As removal in biological rapid sand filters. Water Res. X 1, 100013.
Gude, J.C.J., Rietveld, L.C., van Halem, D., 2016. Fate of low arsenic concentrations during full-scale aeration and rapid filtration. Water Res. 88, 566–574.
Hering, J.G., Chen, P.Y., Wilkie, J.A., et al., 1996. Arsenic removal by ferric chloride. J. Am. Water Work. Assoc. 88, 155–167.
Hiemstra, T., 2013. Surface and mineral structure of ferrihydrite. Geochim. Cosmochim. Acta 105, 316–325.
Hug, S.J., Leupin, O., 2003. Iron-catalyzed oxidation of arsenic(III) by oxygen and by hydrogen peroxide: pH-dependent formation of oxidants in the Fenton reaction. Environ. Sci. Technol. 37, 2734–2742.
Keeley, J., Jarvis, P., Judd, S.J., 2014. Coagulant recovery from water treatment residuals: a review of applicable technologies. Crit. Rev. Environ. Sci. Technol. 44, 2675–2719.
Kitahama, K., Kiriyama, R., Baba, Y., 1975. Refinement of crystal-structure of scorodite. Acta Crystallogr. Sect. B 322–324.
Kraal, P., van Genuchten, C.M., Behrends, T., et al., 2019. Sorption of phosphate and silicate alters dissolution kinetics of poorly crystalline iron (oxyhydr)oxide. Chemosphere 234, 690–701.
Le, A.Van, Muehe, E.M., Drabesch, S., et al., 2022. Environmental risk of arsenic mobilization from disposed sand filter materials. Environ. Sci. Technol. 56, 16822–16830.

Likus, M., Komorowska-Kaufman, M., Pruss, A., et al., 2021. Iron-based water treatment residuals: phase, physicochemical characterization, and textural properties. Materials 14, 3938.
Links, D.A., Rout, K., Mohapatra, M., et al., 2012. Dalton Trans. 1.
Mayer, B.K., Baker, L.A., Boyer, T.H., et al., 2016. Total value of phosphorus recovery. Environ. Sci. Technol. 50, 6606–6620.
Mikutta, C., Frommer, J., Voegelin, A., et al., 2010. Effect of citrate on the local Fe coordination in ferrihydrite, arsenate binding, and ternary arsenate complex formation. Geochim. Cosmochim. Acta 5574–5592.
Muller, S., Behrends, T., van Genuchten, C.M., 2019. Sustaining efficient production of aqueous iron during repeated operation of Fe(0)-electrocoagulation. Water Res. 155, 455–464.
Newville, M., 2001. IFEFFIT: interactive XAFS analysis and FEFF fitting. J. Synchrotron Radiat. 322–324.
Nielsen, S.S., Jakobsen, R., Kjeldsen, P., 2010. Lokalitet nr. 219-3 collstrupgrunden: udredning vedr. Forureningssituationen på og Omkring Grunden 1977–2009.
Ozer, M., 2022. Flotation of antimony ores with high arsenic content. Physicochem. Probl. Miner. Process. 58.
Podgorski, J., Berg, M., 2020. Global threat of arsenic in groundwater. Science 368, 845–850.
Ramsay, L., Petersen, M.M., Hansen, B., et al., 2021. Drinking water criteria for arsenic in high-income, low-dose countries: the effect of legislation on public health. Environ. Sci. Technol. 55, 3483–3493.
Raven, K.P., Jain, A., Loeppert, R.H., 1998. Arsenite and arsenate adsorption on ferrihydrite: kinetics, equilibrium, and adsorption envelopes. Environ. Sci. Technol. 32, 344–349.
Roy, M., van Genuchten, C.M., Rietveld, L., et al., 2022. Groundwater-native Fe(II) oxidation prior to aeration with H2O2 to enhance As(III) removal. Water Res. 223, 119007.
Schwertmann, U., Cornell, R., 1991. Iron Oxides in the Laboratory : Preparation and Characterization. VCH, Weinheim, New York.
Senn, A.C., Kaegi, R., Hug, S.J., et al., 2017. Effect of aging on the structure and phosphate retention of Fe(III)-precipitates formed by Fe(II) oxidation in water. Geochim. Cosmochim. Acta 202, 341–360.
Senn, A.C., Kaegi, R., Hug, S.J., et al., 2015. Composition and structure of Fe(III)-precipitates formed by Fe(II) oxidation in water at near-neutral pH: interdependent effects of phosphate, silicate and Ca. Geochim. Cosmochim. Acta 162, 220–246.
Sheng, A., Liu, J., Li, X., et al., 2020. Labile Fe(III) from sorbed Fe(II) oxidation is the key intermediate in Fe(II)-catalyzed ferrihydrite transformation. Geochim. Cosmochim. Acta 272, 105–120.
Sherman, D.M., Randall, S.R., 2003. Surface complexation of arsenie(V) to iron(III) (hydr)oxides: structural mechanism from ab initio molecular geometries and EXAFS spectroscopy. Geochim. Cosmochim. Acta 67, 4223–4230.
Shi, Y.L., Chen, W.Q., Wu, S.L., et al., 2017. Anthropogenic cycles of arsenic in Mainland China: 1990-2010. Environ. Sci. Technol. 51, 1670–1678.
Sichler, T.C., Becker, R., Sauer, A., et al., 2022. Determination of the phosphorus content in sewage sludge: comparison of different aqua regia digestion methods and ICP-OES, ICP-MS, and photometric determination. Environ. Sci. Eur. 34, 1–15.
Smedley, P.L., Kinniburgh, D.G., 2002. A review of the source, behaviour and distribution of arsenic in natural waters. Appl. Geochem. 17, 517–568.
Sullivan, C., Tyrer, M., Cheeseman, C.R., et al., 2010. Disposal of water treatment wastes containing arsenic - a review. Sci. Total Environ. 408, 1770–1778.
Turner, T., Wheeler, R., Stone, A., et al., 2019. Potential alternative reuse pathways for water treatment residuals: remaining barriers and questions—a review. Water. Air. Soil Pollut. 230.
USEPA, 1992. TCLP, Method 1311, Rev 0. In SW-846: Test Methods For Evaluating Solid Waste, Physical/Chemical Methods. Office of Solid Waste, Washington, DC, 1992.
van Genuchten, C.M., 2022. The enhanced stability of arsenic coprecipitated with magnetite during aging: an XAS investigation. Ind. Eng. Chem. Res.
van Genuchten, C.M., Addy, S.E.A., Pena, J., et al., 2012. Removing arsenic from synthetic groundwater with iron electrocoagulation: an Fe and As K-edge EXAFS study. Environ. Sci. Technol. 46, 986–994.
van Genuchten, C.M., Ahmad, A., 2020. Groundwater As removal by As(III), Fe(II), and Mn(II) co-oxidation: contrasting as removal pathways with O2, NaOCl, and KMnO4. Environ. Sci. Technol. 54, 15454–15464.
van Genuchten, C.M., Etmannski, T.R., Jessen, S., et al., 2022. LCA of disposal practices for arsenic-bearing iron oxides reveals 2 the need for advanced arsenic recovery 1 3. Environ. Sci. Technol. (In-press).
van Genuchten, C.M., Pena, J., Amrose, S.E., et al., 2014. Structure of Fe(III) precipitates generated by the electrolytic dissolution of Fe(0) in the presence of groundwater ions. Geochim. Cosmochim. Acta 127, 285–304.
Villalobos, M., Escobar-Quiroz, I.N., Salazar-Camacho, C., 2014. The influence of particle size and structure on the sorption and oxidation behavior of birnessite: I. Adsorption of As(V) and oxidation of As(III). Geochim. Cosmochim. Acta 125, 564–581.
Voegelin, A., Senn, A.C., Kaegi, R., et al., 2013. Dynamic Fe-precipitate formation induced by Fe(II) oxidation in aerated phosphate-containing water. Geochim. Cosmochim. Acta 117, 216–231.
Waychunas, G.A., Rea, B.A., Fuller, C.C., et al., 1993. Surface-chemistry of ferrihydrite .1. Exafs studies of the geometry of coprecipitated and adsorbed arsenate. Geochim. Cosmochim. Acta 57, 2251–2269.
Webb, S., 2005. SIXPACK: a graphical user interface for XAS analysis using IFEFFIT. Phys. Scr. T115, 1011–1014.
Wovkulich, K., Mailloux, B.J., Lacko, A., et al., 2010. Applied Geochemistry Chemical treatments for mobilizing arsenic from contaminated aquifer solids to accelerate remediation. Appl. Geochem. 25, 1500–1509.
Wu, Y., Zhou, X., Lei, M., et al., 2016. Migration and transformation of arsenic: contamination control and remediation in realgar mining areas. Appl. Geochem.